

Monte Carlo Simulation of Sinusoidally Modulated Superlattice Growth

H. Jeong¹, B. Kahng^{1,2,*}, S. Lee¹, C.Y. Kwak³, A.-L. Barabási¹, and J.K. Furdyna¹

¹ *Department of Physics, University of Notre Dame, Notre Dame, IN 46556*

² *School of Physics and Center for Theoretical Physics, Seoul National University, Seoul 151-742, Korea*

³ *Department of Physics and Center for Advanced Materials and Devices, Konkuk University, Seoul 143-701, Korea*

Abstract

The fabrication of ZnSe/ZnTe superlattices grown by the process of rotating the substrate in the presence of an inhomogeneous flux distribution instead of successively closing and opening of source shutters is studied via Monte Carlo simulations. It is found that the concentration of each compound is sinusoidally modulated along the growth direction, caused by the uneven arrival of Se and Te atoms at a given point of the sample, and by the variation of the Te/Se ratio at that point due to the rotation of the substrate. In this way we obtain a $\text{ZnSe}_{1-x}\text{Te}_x$ alloy in which the composition x varies sinusoidally along the growth direction. The period of the modulation is directly controlled by the rate of the substrate rotation. The amplitude of the compositional modulation is monotonous for small angular velocities of the substrate rotation, but is itself modulated for large angular velocities. The average amplitude of the modulation pattern decreases as the angular velocity of substrate rotation increases and the measurement position approaches the center of rotation. The simulation results are in good agreement with previously published experimental measurements on superlattices fabricated in this manner.

PACS numbers: 68.65.+g, 68.55.Bd, 81.15.H, 61.43.B

Superlattices based on II-VI semiconductors are receiving continued attention as a result of the wide range of new physical phenomena observed in these systems. In particular, several superlattice such as ZnSe/ZnTe [1,2], ZnSe/MgS [3], and ZnSSe/ZnSe [4] have been found interesting because of their potential for applications in optical devices at short wavelengths. Such superlattices are typically fabricated using molecular beam epitaxy (MBE), achieving a periodic structure by repeated openings and closings of the source shutters. This method automatically results in the formation of abrupt interfaces, so that the wells and barriers forming the superlattice are shaped firmly a square pattern.

Growing superlattices with profiles deviating from a square composition profile is desirable for both fundamental research and potential applications. Motivated by this interest, recently a new model of fabricating ZnSe/ZnTe superlattices has been introduced, using the rotation of the substrate as the modulating mechanism instead of shutter opening and closing [1], resulting in sinusoidally modulated superlattices (SMSLs) [1]. The compositional profile of this new structure has been investigated using X-ray diffraction studies, which systematically exhibit a main alloy peak arising from the average $\text{ZnSe}_{1-x}\text{Te}_x$ lattice constant of the alloy, with only one satellite on each side of the main peak, the latter implying that the chemical composition of the alloy x varies sinusoidally along the growth direction [5].

The formation of such SMSLs results from the rotation of the substrate in the presence of a flux inhomogeneity. Such inhomogeneity can arise, e.g., from different distances of the Zn, Se, and Te sources from a given position on the substrate at any one instant. The fact that the period of the sinusoidal modulation is proportional to the period of the rotational motion of the substrate is unambiguously indicated by X-ray measurements, the separation of the superlattice satellites from the main peak indicating that the period grows with the rotation rate. It should be noted that the satellite peak is as narrow as the main alloy peak, indicating that the SMSL structures are of very good quality [1]. The band structure of the SMSL is interesting as well, different from that of *standard* superlattice with

abrupt interfaces [6]. Accordingly, SMSLs are promising for the observation of new optical effects, especially those involving transitions that are forbidden by standard selection rules, and possibly for new optical devices. Even though the physical properties of the SMSL structures are of considerable interest, little has been done so far to firmly establish the process of their formation in any quantitative sense. In this paper, we perform Monte Carlo (MC) simulations reproducing the fabrication process of the SMSLs aiming to understand the basic mechanism contributing to the formation of those structures, helping us to define their structural properties.

Experiment: A $\text{ZnSe}_x\text{Te}_{1-x}$ SMSL was fabricated using a Riber 32 R & D MBE machine, using elemental solid sources, Zn, Se, and Te. Each source cell is located at an approximate distance of 12 cm from the center of the mounting block (“the stage”). The Se and Te sources are located on each side of the Zn source, and the flux rates from the Se and Te are adjusted to make their respective amounts arriving at the center of the stage the same. The relative positions of the sources are shown schematically in Fig.1. The superlattices were grown on (100) GaAs substrates mounted with indium on the molybdenum mounting block, having a diameter of 5.6 cm. The growth of the SMSL was monitored via reflection high electron diffraction (RHEED), whose streaky appearance indicated good layer-by-layer growth throughout the SMSL growth process.

The configuration of the sources shown in Fig.1 produces a nonuniform distribution of flux arriving across the substrate (Se-rich on one side, Te-rich on the other). The consequences of this inhomogeneity manifest themselves clearly when the GaAs substrate has the shape of a long strip (see Fig.1), mounted so that one end of the substrate is much close to the Se source, and the other to the Te source. A strip sample grown in this way without rotation indeed shows a continuous gradient of the concentration along the strip, measured via the X-ray diffraction at various positions along the strip. The maximum difference in the Te and Se concentrations at the two edges of the strip was measured to be approximately

30%, while the concentrations of the two anions at the center of the strip substrate were equal, resulting in a homogeneous $\text{ZnSe}_{0.5}\text{Te}_{0.5}$ alloy.

Simulations: In performing the MC simulations we account for the geometry of the sources and the substrate in the chamber as follows: We choose an anisotropic cell array of $L_x \times L_y = 280 \times 20$, corresponding to 5.6×0.4 cm substrate size, where either ZnSe or ZnTe is deposited on each cell. The size of a unit cell is 0.2×0.2 mm, and $a = 0.2$ mm is taken as the “lattice constant” of the cell. Following this scale, we assume that the sources of Zn, Se, and Te are positioned on a circle with the radius of $600a$ (corresponding to 12cm) from the center of the substrate, so that the ratio between the diameter of the substrate and the distance to the sources is invariant to the experimental values. We use a three-dimensional reference frame whose origin is taken at the center of the substrate, with the growth direction taken as the z direction. x -axis (y -axis) is taken along the longitudinal (transverse) direction of the strip substrate (see Fig. 1). The substrate is then on the $z = 0$ plane, and the sources are located at $S_i = (x_i, y_i, z_i)$, where the index $i = 0, 1$ and 2 stands for Zn, Se, and Te, respectively. Thus, for example, the Zn source is located at $S_0 = (-r_0 \sin 11^\circ, 0, r_0 \cos 11^\circ)$, with $r_0 = 600a$. In the actual experiment the positions of the sources are fixed in the (x, z) -plane, while the substrate rotates with the angular velocity ω . In our simulations we fix the substrate and equivalently rotate the sources in the reverse direction with the same frequency ω . The epilayer height $h(x, y)$ at any time is defined as the height of the top of the epilayer at the position (x, y) on the substrate. The flux from the source i at the position $P = (x, y, h)$ on the surface is given by

$$F_i = \frac{f_i \cos \theta_i}{4\pi r_i^2} = \frac{f_i |z_i - h|}{4\pi r_i^3}, \quad (1)$$

where f_i is the emission rate of the source i , r_i is the distance between the source and position P , and θ_i is the polar angle between the vertical line of the source i and the line connecting the source i and the point P . The emission rates f_i of the Se and Te sources are adjusted so as to make the Se and Te fluxes at the center of the substrate identical. In

simulations, we choose $f_1 = 1.0$. Accordingly, $f_2 = \cos(33^\circ)/\cos(11^\circ)$, leading to the total emission rate $f_1 + f_2 \approx 1.854$.

The MC simulations are performed using discretized time, where a unit time step is taken to be $\Delta t = 1/[(f_1 + f_2)L_xL_y]$. Then the time for one monolayer to grow is $T_m = 1/(f_1 + f_2)$. At each time step Δt , the following calculations are carried out. First, we choose a single cell among the 280×20 cells at random, and a single molecular species of either ZnSe or ZnTe is deposited on that cell. Second, the selection of either ZnSe or ZnTe for the deposition is determined according to the probability proportional to the ratio of the two fluxes arriving at the selected cell from the Se and Te sources. Third, the selected molecular species is allowed to diffuse into the lowest-lying cell within the nearest-neighboring cells. If there are more than one lowest cells, then one of those cells is randomly selected with equal probability. The substrate is then allowed to rotate with an angle $\Delta\theta = \omega\Delta t$, after which the above three MC simulation steps are repeated.

The first three MC simulation steps incorporated in our model are based on the following physical reasoning: First, since each cell has a linear size of 0.2 mm, which is enormous on the atomic scale, in the experiment a large number of compound molecules can be deposited within a single cell. However, it is not feasible to deal with such large numbers of molecules in the simulations. Thus in the MC simulations we deal with a single representative of the large number of compound molecules in a unit cell. Consequently, molecular species in the simulations represent a coarse-grain particle, comprised of a large number of molecules on the atomic scale [7]. However, in order to see the modulation pattern along the z direction, we use a disproportionate short unit length scale for the z direction. Specifically, the height of the unit cell is taken as small as 5×10^{-6} times the lateral size of the cell, so that the upward growth of the superlattice is simulated in terms of 1024 layers. This corresponds to a height of $\sim 1\mu m$, the thickness of superlattices fabricated in a typical experiment.

The second step is based on the assumption that the Zn element is supplied in sufficient amount to react with both Se and Te, and the reaction rates of the Zn-Se and Zn-Te are identical, even though in reality the reaction rate of Zn-Se is known to be slightly higher than that of the Zn-Te. When the reaction rates are assumed to be identical, a coarse-grained species can be selected as the “majority alloys” within a given cell, proportional to the ratio of the incoming fluxes.

For the third step, we consider the following situation: when Zn, Se, and Te atoms arrive at the epilayer surface, they have sufficient energy to diffuse into the lowest-lying sites within the diffusion length, followed by nucleation, and they then remain at these most stable sites. In the simulation, since we deal with the coarse-grain particles instead of individual adatoms, their collective behavior is very complicated. In reality, the collective motion is not contained within the cell, but mass flow occurs across the boundary between neighboring cells. Accordingly, to mimic this mass flow, we allow incoming coarse-grain particles to diffuse to the nearest neighboring cells. This does not necessarily imply that particles diffuse the distance of a coarse grain cell. It is just the most efficient way to simulate mass transfer without considering all the details of the diffusion process. This diffusion process moderates the height fluctuation that would arise from a completely random deposition process, and enables the surface to grow in a layer-by-layer growth mode. Such local diffusion process was first introduced in a model proposed by Family [8], which results in the reduction (smoothing) of the surface height fluctuations, *i.e.*, the surface of the material simulated in this way exhibits the layer-by-layer growth up to some characteristic thickness, after which the height fluctuation begins to increase with time [9]. Our simulations are thus limited to a characteristic thickness, restricted by the above layer-by-layer growth requirement. Although the above model of the eventual emergence of surface roughness is universal, being independent of the diffusion length, in our simulation we restrict the diffusion length to the lattice constant of the unit cell. It is worth noting that the MC simulations using coarse-grain particles lead to the same result as that obtained with a single-particle model in the problem of the

island density distribution in monolayer epitaxial growth [7].

Simulation results: A typical superlattice generated by the MC simulations just described is shown in Fig.2a. This representation does not by itself show a clear separation between the predominantly ZnSe- and ZnTe-rich regions. In order to increase the contrast in the modulation pattern, in Fig.2b we replot the same data, but with the alloy density averaged along the y direction in each (x, z) point. The modulation pattern can now be seen distinctly. To bring out the modulation more clearly, we next consider the density profile of one compound (ZnSe), as a function of z , measuring the concentration of ZnSe within a square of $\ell_x \times \ell_y = 10a \times 10a$, located at the edge of the substrate.

As shown in Figs.3a and 3b, the concentration exhibits two different types of sinusoidally-oscillating behavior. When the angular velocity ω of the rotation of the substrate is small, the amplitude of the modulation pattern is invariant for different heights z (Fig.3a). On the other hand, for large ω , the envelope of the modulation pattern is itself modulated (Fig.3b). The latter behavior occurs when the period of the rotation of the substrate $T_r = 2\pi/\omega$ is short, and is not integer-multiple of the time needed to deposit one monolayer $T_m = 1/(f_1 + f_2)$. While the epilayer grows by one monolayer, the substrate rotates with the angle $\theta_m = \omega T_m$. When $\theta_m \neq 2\pi/n$ for integer n , the second type of the density profile occurs; when ω is not large enough, the top layer is only partially covered during the period of one revolution. The fraction of covered cells changes as the revolution proceeds further. When $\theta_m \neq 2\pi/n$, the fraction of covered cells on the top layer after n revolutions of the substrate is not the same as the one before. Let n be the number of monolayers between two successive peaks in the density profile as seen in Fig.3b. Then since the fractions of covered cells before and after the n revolutions are not equal, the densities of one compound at the positions of the two peaks are different, too.

In particular, when the ratio between the two time scales $T_r/T_m = (2\pi/\omega)(f_1 + f_2)$

can be written as a rational fraction k/ℓ , where k and ℓ are integers, the substrate returns to the same orientation with the same fraction of covered cells after ℓ revolutions of the substrate, during which k monolayers are deposited. Thus, the amplitude of the envelope is recovered to its value after ℓ revolutions of the substrate. For example, when $\omega = 3.0$ and $f_1 + f_2 \approx 1.854$, the ratio becomes $T_r/T_m \approx 31/8$. Therefore the period of envelop modulation is 8 revolutions, during which 31 monolayers of material is deposited, as shown in Fig.3b.

Next, we investigated the power spectrum of the density profile, corresponding to the x-ray scattering intensity observed experimentally. We found that the power spectrum shows a single peak located at ω_p as shown in Fig.4, regardless of the two types of the density profile. The location of the single peak is proportional to the angular velocity of the substrate rotation, as shown in Fig.5. The occurrence of the single peak in the power spectrum, even for the case when the modulated envelope is present, implies that there exists only one generic frequency in the system. This generic frequency is equivalent to the angular frequency of the rotation of the substrate. To understand why only a single peak occurs even for the case with the modulated amplitude, we in Fig.6 replot the data of in Fig.3a using three-monolayer unit rather than one-monolayer unit used in Fig.3a. The amplitude of the modulation is itself modulated, even though Fig.3a and Fig.6 are drawn from identical data. Since the two density profiles are actually identical, their power spectra would be the same, exhibiting one single peak, located at the position corresponding to the angular frequency ω , which is $\omega = 1.0$. Next, when x -axis is rescaled by $1/3$ in Fig.6, the density profile becomes equivalent to that in Fig.3b for $\omega = 3.0$, but the amplitude is reduced. Therefore, it is natural to expect that the power spectrum of the density profile in Fig.3b exhibits a single peak instead of the two peaks that might intuitively be expected to result from the beats of the periods of rotation of the substrate and of the amplitude modulation.

Finally, we studied the intensity of the power spectrum, and found that it depends on the

angular velocity of the substrate ω and the location of the square where the measurement was taken. Here, we first examined the intensity as a function of the angular velocity ω . As shown in Fig.7, it is found that the modulation intensity decreases as the angular velocity increases, reflecting that the flux inhomogeneity becomes weaker as the angular velocity increases. Thus, while we can obtain effective superlattices with shorter periods we increase the angular velocity of the rotation of the substrate, the flux inhomogeneity incident on a given cell becomes weaker, lowering the the quality of the superlattice fabricated with higher angular velocity. Second, we examined the amplitude of the modulation pattern as a function of the location where the measurement was taken. As shown in Fig.3a, for a given angular velocity, the amplitude gradually decreases to zero as the measurement position approaches the center of the substrate. The amplitude has extrema at the edges of the substrate, which for our parameters has values ≈ 0.62 and ≈ 0.39 for the ZnSe content, in reasonable agreement with the experimental results.

In conclusions, we have performed MC simulations for the fabrication of $\text{ZnSe}_{1-x}\text{Te}_x$ SMSL in which the composition x that varies sinusoidally. It is found that the modulation of the density of ZnSe or ZnTe along the growth direction is caused by both the inhomogeneity of the fluxes from the Zn, Se, and Te sources incident at a given point of the substrate and by the rotation of that substrate. The modulation of the structure is displayed in Figs.2 and 3, showing the alternative occurrence of gradually-changing ZnSe-rich and ZnTe-rich domains along the growth direction, instead of sharp interfaces between these domains. When the rate of substrate rotation is slow (fast), the amplitude of the modulation pattern is monotonic (modulated). It is found that the estimated period of the modulation pattern is proportional to the rate of rotation. The mean modulation amplitude decreases as the rate of rotation of the substrate increases, and also as the measurement position approaches the center of the substrate.

This work was supported by the U.S. DOE Grant 97ER45644 and the Korean Research Foundation (Grant No. 99-041-D00150).

REFERENCES

- * Author to whom correspondence should be addressed. Email: kahng@phya.snu.ac.kr
- [1] P.M. Reimer, J. R. Buschert, S. Lee, and J.K. Furdyna, Phys. Rev. B **61**, 8388 (2000).
- [2] S. Lee, U. Bindley, J.K. Furdyna, P.M. Reimer, and J.R. Buschert, J. Vac. Sci. Technol. B **18**, 1518 (2000).
- [3] K.T. Obinata, I. Suemune, H. Kumano, and J. Nakahara, Appl. Phys. Lett. **68**, 844 (1996).
- [4] K. Shahzad, D.J. Olego, and C.G. Van de Walle, Phys. Rev. B **38**, 1417 (1988).
- [5] P.F. Fewster, Semicond. Sci. Technol. **8** 1915 (1993).
- [6] G. Yang, S. Lee, and J.K. Furdyna, Phys. Rev. B **61**, 10,978 (2000).
- [7] D.E. Wolf, in *Scale Invariance, Interfaces, and Non-Equilibrium Dynamics*, edited by A. McKane *et al.* (Plenum, New York, 1995), pp. 215-248.
- [8] F. Family, J. Phys. A **19**, L441 (1986).
- [9] S. Park, H. Jeong, and B. Kahng, Phys. Rev. E **59**, 6184 (1999).

FIGURE CAPTIONS

- Figure 1. Schematic view of the MBE chamber, showing the relative positions of the sources and the size of the substrate.
- Figure 2. “Snapshot” of the SMSL structure for $\omega = 0.5$ rad/sec with (a) raw MC data, and (b) processed data using the averaged density along the y direction, as discussed in the text.
- Figure 3. The profile of the density of the ZnSe compound as a function of height z for $\omega = 0.5$ (a) and 3.0(b). In (a), the data with the largest amplitude of modulation (solid line), median (dotted line), and smallest amplitudes (dashed line) are selected from the squares of $10a \times 10a$ ($a = 0.2\text{mm}$), whose centers are located at $(x, y) = (-135a, 0)$, $(-75a, 0)$, and $(-45a, 0)$, respectively. The symbol (\diamond) denotes the densities obtained at one-monolayer steps T_m . The data are averaged over 100 configurations.
- Figure 4. The power spectrum of the density profile of the ZnSe compound for $\omega = 1.0$ and 3.0 (inset). We perform a Fourier transform of the density profile with 1024 data points, resulting in the frequency ranged from 1 to 512.
- Figure 5. Plot of the estimated location of the Fourier peak in the power spectrum versus the rate of substrate rotation, ω , showing that only the ω -parameter determines the power-spectrum distribution.
- Figure 6. A plot of the density profile for Fig.3a using three-monolayer steps (\diamond).
- Figure 7. Modulation amplitude of SMSL (in terms of ZnSe density) as a function of the rate of substrate rotation ω . For highest values of ω the short-period SMSL gradually transforms into a homogeneous alloy.

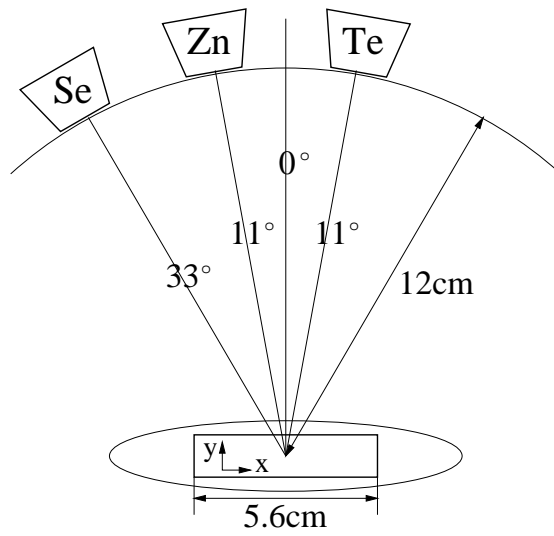
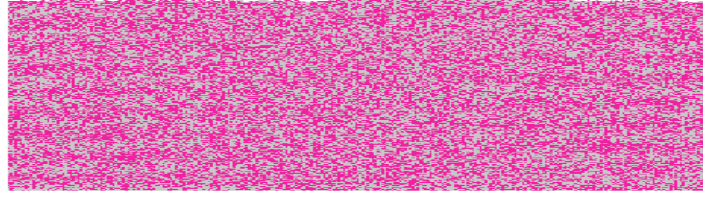
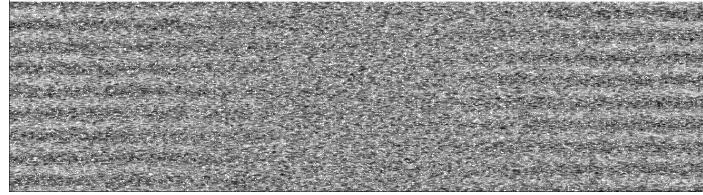


Figure 1. H. Jeong *et al.* “Monte Carlo Simulation of Sinusoidally Modulated Superlattice Growth”



(a)



(b)

Figure 2. H. Jeong *et al.* “Monte Carlo Simulation of Sinusoidally Modulated Superlattice Growth”

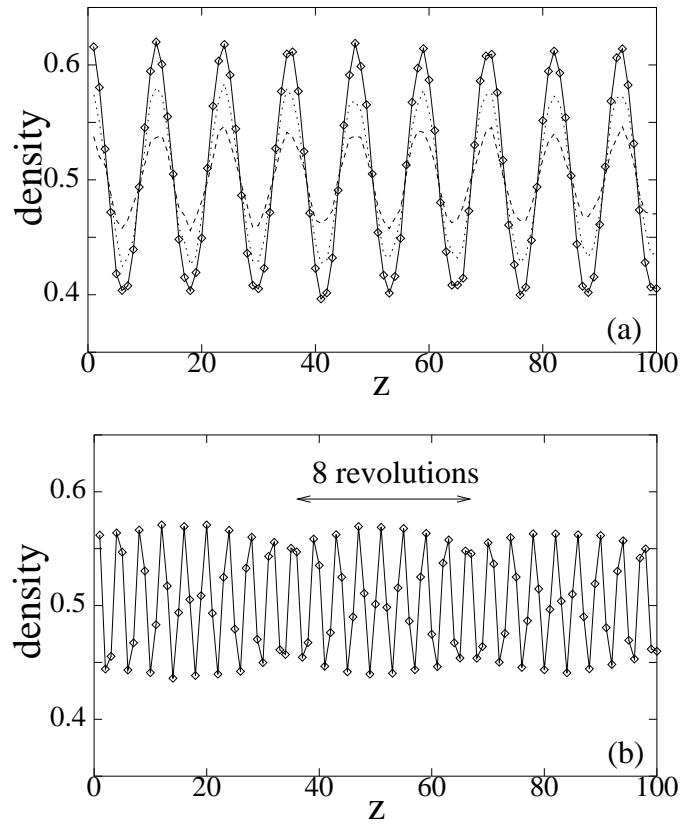


Figure 3. H. Jeong *et al.* “Monte Carlo Simulation of Sinusoidally Modulated Superlattice Growth”

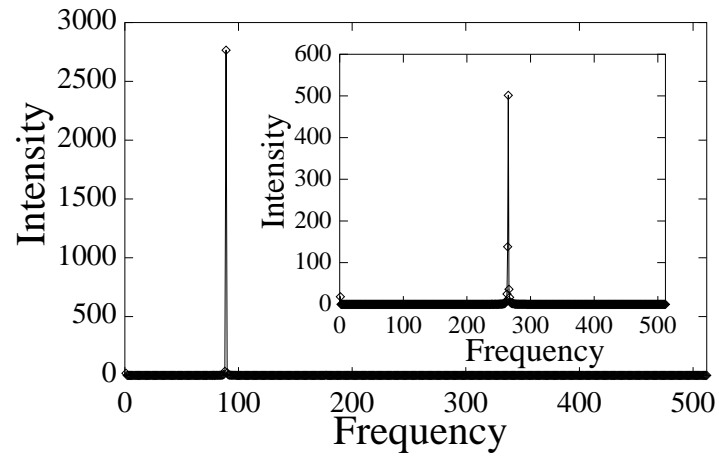


Figure 4. H. Jeong *et al.* “Monte Carlo Simulation of Sinusoidally Modulated Superlattice Growth”

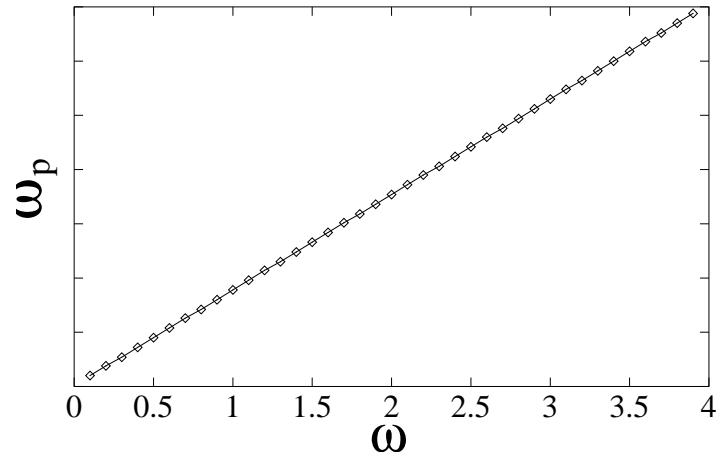


Figure 5. H. Jeong *et al.* “Monte Carlo Simulation of Sinusoidally Modulated Superlattice Growth”

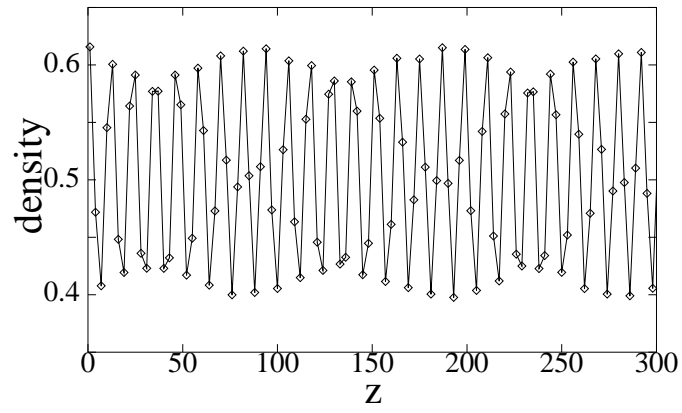


Figure 6. H. Jeong *et al.* “Monte Carlo Simulation of Sinusoidally Modulated Superlattice Growth”

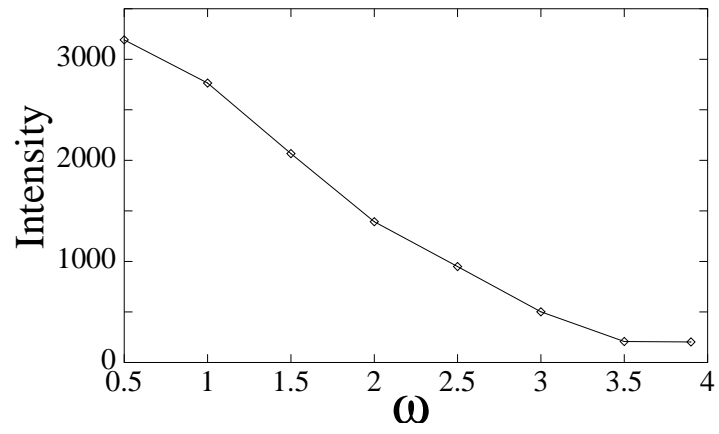


Figure 7. H. Jeong *et al.* “Monte Carlo Simulation of Sinusoidally Modulated Superlattice Growth”